ACS APPLIED MATERIALS & INTERFACES

RESEARCH ARTICLE

www.acsami.org

Core−Shell Structured Carbonyl Iron Microspheres Prepared via Dual-Step Functionality Coatings and Their Magnetorheological Response

Fei Fei Fang,[†] Ying Dan Liu,[†] Hyoung Jin Choi,[†,*] and Yongsok Seo[‡,*]

[†]Department of Polymer Science and Engineering, Inha University, Incheon 402-751, Korea

[‡]Intellectual Textile System Research Center (ITRC) and School of Materials Science and Engineering, College of Engineering, Seoul National University, Seoul 151-744, Korea

Supporting Information

ABSTRACT: The dispersion stability of soft magnetic carbonyl iron (CI)-based magnetorheological (MR) fluids was improved by applying a unique functional coating composed of a conducting polyaniline layer and a multiwalled carbon nanotube nest to the surfaces of the CI particles via conventional dispersion polymerization, followed by facile solvent casting. The coating morphology and thickness were analyzed by SEM and TEM imaging. Chemical composition of the polyaniline layer was detected by Raman spectroscope, which also confirmed the coating performance successfully. The influence of the functional coating on the magnetic properties was investigated by measuring the MR performance and sedimentation properties using a vibrating sample magnetometer, rotational rheometer, and Turbiscan apparatus. Improved dispersion characteristics of the MR fluid were observed.

KEYWORDS: magnetorheological fluid, carbonyl iron, polyaniline, carbon nanotube, magnetic particle

1. INTRODUCTION

Magnetorheological (MR) fluids consisting of soft magnetic particles dispersed in nonmagnetic fluids are regarded as "smart" or "intelligent" engineering materials because they flow in the absence of a magnetic field but immediately solidify under an applied external magnetic field. The rheological properties (yield stress, apparent viscosity, and storage modulus) can vary significantly with the magnetic field strength, permitting fine-tuning of the material behavior.[1−16] MR fluids, along with the electrically analogous electrorheological (ER) fluids,[17−19] have attracted considerable attention because they are applicable in, for example, dampers, torque transducers, or polishing devices.[20,21]

The excellent magnetic properties and particle sizes of soft magnetic carbonyl iron (CI) microsphere-based MR fluids have attracted attention in both scientific and industrial studies.[22−25] Application of CI-based MR fluids in MR devices requires improvements in the fluid properties because sedimentation problems caused by the large density mismatch between the CI particles and the oil medium hampers MR device operation as well as their redispersion. Various strategies (introducing submicrometer-sized additives or polymer coating technologies) have been tested to prevent CI particles from coming into contact or to decrease the particle density, thereby reducing sedimentation. The addition of submicrometer-sized fillers (multiwalled carbon nanotube (MWCNT), graphite nanotubes, fumed silica, and organoclay) is an effective method for increasing dispersion stability by providing a physical layer that inhibits direct contact among CI particles to improve the stability of the MR fluid.[26−28] However, because the size, morphology, and affinity of the additive toward the CI particles can affect the fluid properties, polymer coating techniques appear to be the best option for stabilizing MR fluid suspensions. Applying polymer coatings to CI particle surfaces introduces favorable core−shell structures and decreases the density of CI/polymer composite particles.[22,29,30]

The coating of polymers onto CI particle surfaces is not a facile process, despite the use of versatile functional grafting agents. Failing to select an optimal grafting agent can yield a thin coating layer that may be prone to failure. The mole ratio between monomers, the stirring rate, the initiator or stabilizer, and the reaction temperature also play critical roles in the shell morphology. Recently, we employed MWCNTs to wrap CI particles because MWCNTs have a density comparable to that of polymers but they display better magnetic properties due to the presence of residual iron catalyst used in the MWCNT synthesis. With the aid of ultrasonication and grafting reagents, a dense MWCNT nest formed on the surface of CI particles to produce a rough surface. The intensity and duration of ultrasonication was adjusted to provide the desired thickness of MWCNT layers.[31] To improve the sedimentation problems associated with CI-based MR suspensions, we used a two-step coating process to introduce a conducting polyaniline (PANI) shell and a MWCNT nest on the CI particle surfaces, rather than using a single polymer or MWCNT layer coating. Note that recently sequential coating with polymer and MWCNT has been reported.[32,33] Scheme 1 shows the synthesis process for producing MWCNT/PANI/CI composite particles.

The PANI shell was selected for several reasons. Unlike the synthesis of some polymers (such as poly(methyl methacrylate) or polystyrene), which are sensitive to the stirring rate during

Received: June 2, 2011
Accepted: August 4, 2011
Published: August 04, 2011

Scheme 1. Schematic Diagram of the Synthesis Process for Producing MWCNT/PANI/CI Composite Particles

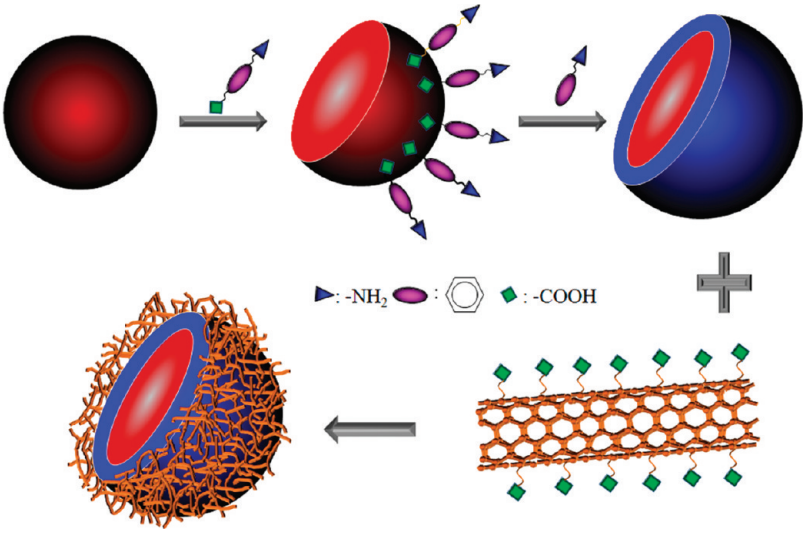

polymerization,[34] PANI forms a reproducible shell morphology on spherical core polymer particles, independent of the stirring rate.[35−37] As shown in Scheme 1, the conducting PANI shell was loaded by modifying the hydrophilic CI core surface with a smart grafting reagent that included one carboxyl moiety and one amino moiety: para-amino benzoic acid (PABA). The dopant selected for the synthesis of the conducting PANI is unusual. Dodecylbenzene sulfonic acid (DBSA) was selected as a dopant rather than strong acids (HCl or H_2SO_4) frequently used as dopants in the synthesis of PANI to prevent corrosion of the CI particles. It is both a dopant for producing conducting PANI and a surfactant.[38−42] Although the polymer coating method reduced the density dispersion, it also produced smooth surfaces on the pure CI particles, which can promote sedimentation. A second step was introduced, involving a facile solvent casting method recently reported by Yi et al.,[43] who fabricated unique MWCNT cages. We constructed a MWCNT nest on the PANI-coated CI particles to provide a rough surface, which was expected to slow the settling speed.[43] The core−shell structured morphology was analyzed, and the effects of this structure on the magnetic properties, MR behavior, and dispersion stability were investigated.

2. EXPERIMENTAL SECTION

2.1. Synthesis of PANI-Coated CI Particles. A PANI shell of thickness 80 nm was fabricated by conventional dispersion polymerization methods using aniline. In a general synthesis route, poly(vinyl alcohol) (PVA-1700, DC Chemical Co. Ltd., Korea), dodecylbenzene sulfonic acid (DBSA, Sigma-Aldrich Co. Ltd. USA), aniline (DC Chemical Co. Ltd., Korea), and ammonia peroxide (APS, Dae Jung Chemicals & Metals Co. Ltd., Korea) were used as the stabilizer, dopant, monomer, and initiator, respectively. Initially, soft magnetic CI particles (8.50 g) (CD grade, BASF Germany, average particle size: 4.25 μm; density: 7.91 g/cm^3) were mixed with a predispersed solution of PABA (2.0 g) in DI water (250.0 g) with ultrasonication. After 30 min, the excess PABA was removed by washing with excess DI water. PABA-modified CI particles were then mixed with the initiator APS (13.04 g) in DI water (80.0 g) and ultrasonicated for 15 min. A homogeneous dispersion of PVA (20.0 g) in DI water (500.0 g) was prepared in a 3-neck round reactor (1 L) followed by cooling to 5 °C. After transferring the mixture of PABA-modified CI particles and the APS dispersion to the reactor, 150 g of a solution containing water, aniline (4.25 g), and DBSA (16.33 g) was added dropwise. The solution was maintained at 5 °C for 24 h under vigorous stirring. A high stirring rate (rpm: 450) was sustained to avoid sedimentation due to high density (7.91 g/cm^3) of CI particles. The resulting dark green precipitate was washed with excess DI water and acetone using a magnet to retain the particles, and the powder was dried in a vacuum oven at 60 °C for 24 h.

2.2. Second Coating Layer of MWNT. A dense MWCNT nest was constructed on the surfaces of the PANI/CI composite particles via a facile solvent casting methodology. Initially, PANI/CI composite particles (6.0 g) were added to 20.0 g of a homogeneous dispersion of carboxylic acid-functionalized MWCNTs (1.0 g) in water with vigorous stirring. This mixture was rapidly poured into 100 mL of a preheated silicone oil bath (90 °C KF-96, 100 cs, Shin Etsu) to form a water-in-oil (W/O) emulsion system. A high stirring rate (rpm: 700) was applied with heating (90 °C) to remove residual water by evaporation. The suspension was slowly cooled to room temperature, the MWCNT-wrapped PANI/CI particles were extracted with excess acetone, and the particles were dried completely in an oven for 24 h.

2.3. Characteristics. The surface morphologies of the pure CI particles, PANI/CI particles, and the MWCNT/PANI/CI particles were observed using scanning electron microscopy (SEM, S-4200, Hitachi Japan). Elemental analysis was obtained from the X-ray energy dispersive spectra (EDS) using an attached EDAX (coupled with Hitachi S-4200) spectrometer. Cross-sectional views of the PANI/CI particles were studied by transmission electron microscopy (TEM, Philips CM200). TEM cross-sectional samples were prepared by molding the particles dispersed in an epoxy bath, nanoscale cutting the molded sample using an ultramicrotome (UMT), and depositing the samples on a copper grid. The composition of the PANI layer was analyzed by Raman spectroscopy recorded using a RFS 100/S Bruker spectrometer with 1064 nm radiation from an air-cooled diode-pumped Nd:YAG laser. The laser beam was focused on the sample in the front compartment at a laser power of 100 mW. Magnetic measurements were conducted on the powder at room temperature using a vibrating sample magnetometer (VSM, Lakeshore 7307, USA) with a maximum magnetic field of 650 A/m. The density of the particles was checked by pycnometry (AccuPyc 1330).

MR characterization was conducted by dispersing pure CI particles and MWCNT/PANI/CI particles in silicone oil (KF-96, 100cs, Shin Etsu, Japan) at a given concentration (20 vol%) to permit comparison.

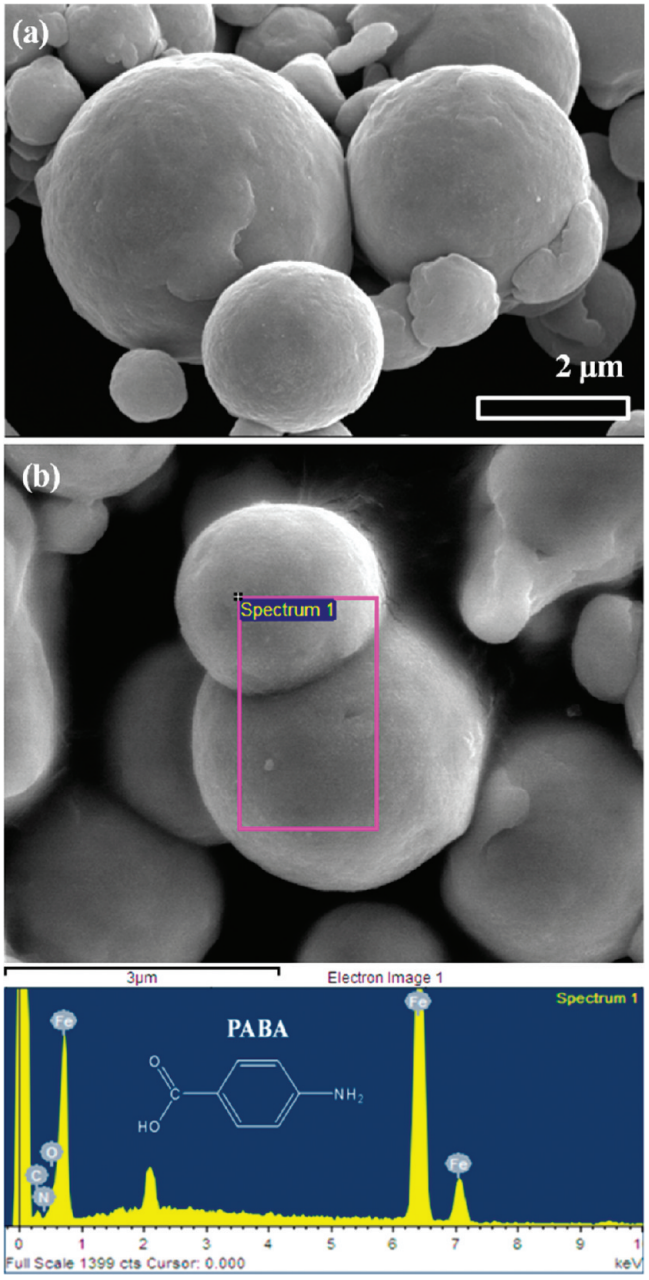

Figure 1. SEM image of (a) pure CI particles and (b) PABA-modified CI particles with EDS spectra.

MR performances were investigated using a rotational rheometer (Physica MCR 300, Stuttgart, Germany) equipped with an MR device (MRD 180, Physica). The parallel-plate measuring system included nonmagnetic metals to prevent introduction of radial magnetic force components on the shaft of the measuring system. A Turbiscan lab expert system (Formulation, France) was used to measure light transmission through the suspension as a function of time along the *y*-axis sample coordinates. These measurements indicated the stability of the suspension.

3. RESULTS AND DISCUSSION

3.1. Surface Morphologies, Chemical Composition, and Magnetic Properties. The particle morphology was investigated at each step. The pristine CI particles, shown in Figure 1a, exhibited smooth surfaces and a polydisperse size distribution. Figure 1b indicates that the smooth CI particle surfaces were preserved after modification with PABA under ultrasonication. The composition of the surface of the PABA-modified CI particles was examined by element analysis, in which an electron beam was focused on randomly selected regions on the PABA-modified CI particle surfaces. The EDS spectra of the PABA-modified CI particles (the inset shows the chemical structure of PABA) indicated the presence of organic elements with strong peak intensities (carbon, nitrogen, and oxygen), originating from the PABA. Considering that the PABA-modified CI particles were washed away with DI water, these organic species indicated the successful modification of CI particle surfaces with PABA.

Formation of the PANI polymer yielded distinct changes in the surface morphology, as indicated in Figure 2a. The full scale images showed that the CI particles were covered with a thick shell, and some particles formed aggregates. A magnified view (Figure 2b) clearly indicated that the morphology of the PANI/CI particles was rough, unlike the smooth surfaces of the pure CI particles. The shell was examined by EDS (see Figure S1 in the Supporting Information), which indicated the presence of high-intensity organic species peaks corresponding to carbon, nitrogen, oxygen, and sulfur. The increased intensity of N, O, and S, combined with a decreased intensity of Fe, demonstrated that the CI particles were successfully coated with a PANI shell. The coating thickness could be observed by TEM, in which the cross sections of the synthesized PANI/CI composite particles were imaged, as shown in Figure 2c. The inset shows a TEM image of pure CI particles, which displayed fairly smooth surfaces. The PANI-coated CI particle images showed an internal black center representing the CI core and a light outer shadow representing the PANI shell. The thickness of the PANI shell was about 80 nm. This result indicated the successful coating with a PANI shell. Figure 2d shows the morphology of the MWCNT-wrapped PANI/CI particles obtained using the solvent casting method. The particle surfaces were fairly rough, and a mass of the MWCNTs compactly covered the surfaces. The facile W/O emulsion method was employed to produce a dense MWCNT nest. Spherical morphologies were favored by the evaporation of water droplets dispersed in an oil bath heated at high temperatures with rapid stirring. The spherical morphology of the PANI/CI particles was preserved at the surface of the PANI shell. The two-step coating method thereby converted pure CI particles with smooth surfaces into particles with rough surfaces, which are expected to reduce sedimentation in CI-based MR fluids.

The chemical composition of the PANI shell was investigated by Raman spectroscopy. Figure 3a shows the resonance Raman spectra of pure CI particles, PANI-coated CI particles, and pure PANI. For comparison purposes, the Raman spectrum of the PANI residue collected from the reactor after polymerization was also examined. No peaks were observed for the pure CI particles. PANI-coated CI particles exhibited peaks that were characteristic of PANI polaronic units under 1064.0 nm laser excitation.[44−46] The presence of polaronic bands at 1174 cm^{-1} and 1373 cm^{-1} in the spectra of the PANI/CI particles and the PANI residue indicated that these samples were doped with DBSA. The band at 1174 cm^{-1} was ascribed to C−H deformations, and the band at 1505 cm^{-1} corresponded to a C═N stretching mode. The ratio of the intensity of the band corresponding to C−N+ at 1373 cm^{-1} and the band corresponding to an aromatic −C−C− stretch at 1600 cm^{-1} was about 1. This result suggested that both

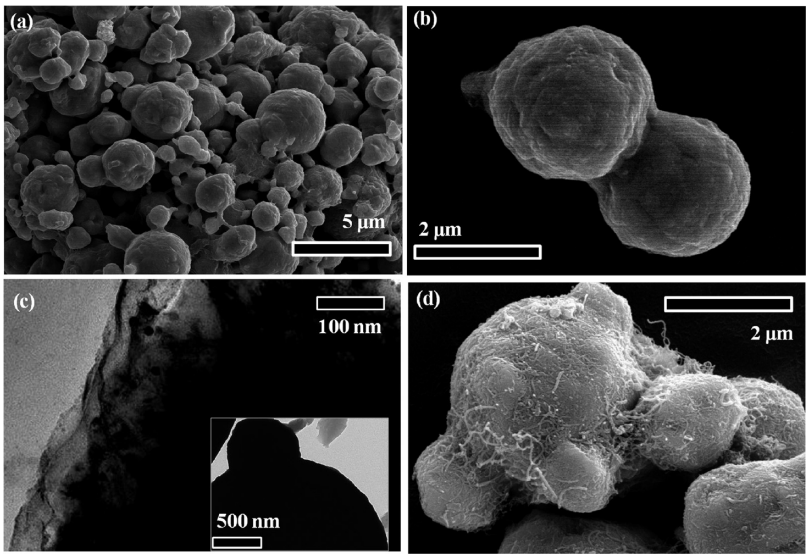

Figure 2. SEM images of PANI coated CI particles in (a) a full view and (b) a locally magnified view; (c) TEM image of PANI coated CI particles; the inset image is TEM view of pure CI particles; (d) SEM image of MWCNT wrapped PANI/CI magnetic particles.

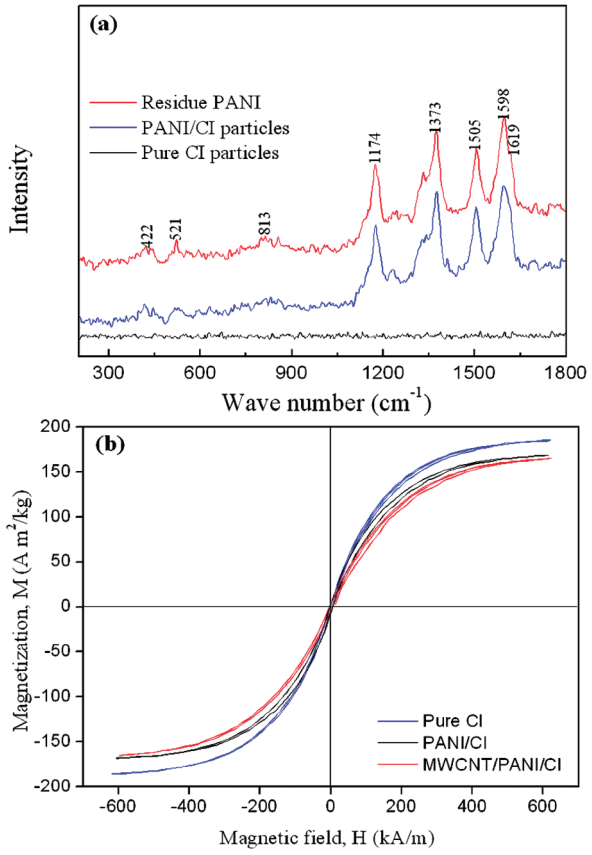

Figure 3. (a) Raman spectra of powder samples of residue PANI (red line), PANI/CI particles (blue line), and pure CI particles (black line); (b) VSM data of pure CI particles (blue line), PANI/CI particles (black line), and MWCNT/PANI/CI particles (red line).

the PANI residue and the coated PANI shell contained emeraldine salts, which is a conducting form of PANI.

The magnetic hysteresis loops of the MWCNT/PANI/CI particles, PANI/CI particles, and pure CI particles in the powder state, measured in the magnetic field range from −625 to 625 kA/m, are shown in Figure 3b. The saturation magnetization (the maximum possible magnetization of a material obtained from VSM) of pure CI particles differed from that of the coated CI particles. As shown in Table 1, the PANI coated CI particles displayed a 12.8% reduction in the saturation magnetization from 188 of the pure CI particles to 164 A m^2/kg upon introduction of the nonmagnetic PANI shell. However, after loading of a dense MWCNT nest via the solvent casting method, the saturation magnetization decreased slightly to 161 A·m^2/kg. This result suggested that the PANI shell coating reduced the magnetic properties, but wrapping with the MWCNT nest did not significantly influence the magnetic properties. The suspension density was measured by pycnometry. As shown in Table 1, the density was reduced from 7.91 g/cm^3 for pure CI particles to 6.70 g/cm^3 for MWCNT/PANI/CI particles and 6.89 g/cm^3 PANI/CI particles. This result agreed with the saturation magnetization measurements. Slight difference between that from saturation magnetization and that from particle density might come from the negligible experimental error from each measurement.

Table 1. Saturation Magnetization and Density for Pure CI, PANI/CI, and MWCNT/PANI/CI Particles

	pure CI	PANI/CI	MWCNT/PANI/CI
saturation magnetization (A m^2/kg)	188	164	161
density (g/cm^3)	7.91	6.89	6.70

3.2. MR Performances. The MR fluid properties were characterized at magnetic field strengths ranging from 0 to 343 kA/m under both rotational and oscillatory tests. Flow curves were collected using a conventional controlled shear rate (CSR) mode, which is the most common way to determine the dynamic yield stress.[47,48] The shear rate varied from 0.01 to 500 s^{-1} on a log scale because shear rates that are too high can result in sample expulsion from the space between the parallel disks. The measuring point duration of each shear rate sweep varied from an initial duration of 15 s to a final duration of 1 s, on a log scale.

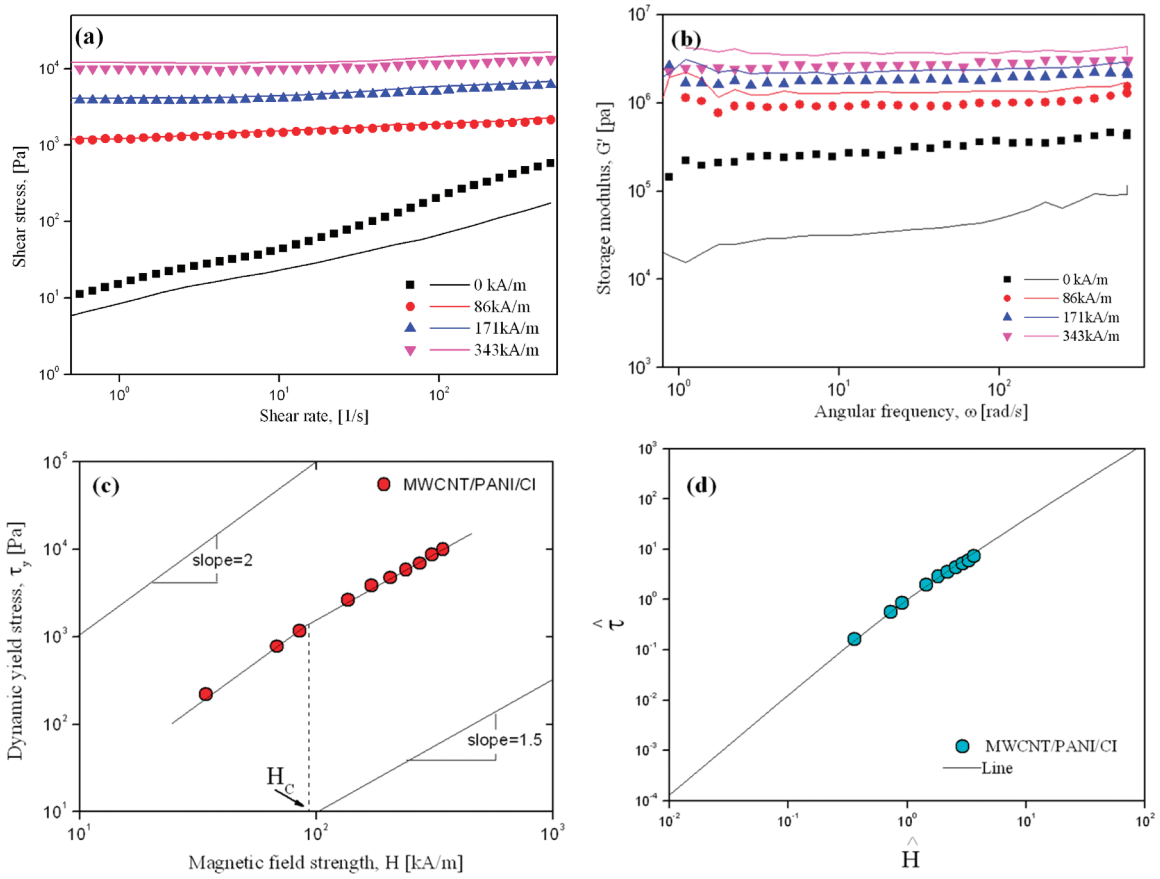

Figure 4. (a) Typical flow curves and (b) oscillatory graph of pure CI suspension (lines) and MWCNT/PANI/CI suspension (symbols); (c) replotted dynamic yield stress graph as a function of magnetic field strength and (d) plot of $\hat{\tau}$ vs $\hat{H}$ for MWCNT/PANI/CI suspension.

Figure 4a shows that the MWCNT/PANI/CI composite particle suspension displayed a higher shear stress relative to that of the pure CI-based suspension in the absence of a magnetic field. In contrast with the pure CI suspension, the MWCNT/PANI/CI suspension displayed a nonzero yield stress at low shear rates. This interesting observation could be explained in terms of the unique morphology of the MWCNT/PANI/CI particles. The two-step CI microsphere coating process produced a rough MWCNT/PANI/CI particle surface composed of numerous MWCNTs. The surface roughness was expected to increase the friction among particles relative to the pure CI particles. Under an external shear field, these rough particles inevitably came into contact, and the adsorbed MWCNTs produced flocculation by bridging the gap between adjacent CI particles,[49] thereby enhancing the rheological properties (apparent viscosity, yield stress, and modulus).

Under an applied magnetic field, the rheological properties of the systems displayed a similar dependence on the magnetic field strength and a wide plateau over the shear rates. The wide plateau was attributed to the dipole−dipole interactions among adjacent magnetic particles. Unlike the behavior obtained in the absence of a magnetic field, the MWCNT/PANI/CI suspension yielded a lower shear stress than a pure CI suspension under a given magnetic field strength. The dynamic yield stress collected at the intersection with the shear stress axis decreased from 1.226, 4.170, and 12.10 kPa to 1.162, 3.88, and 10 kPa at magnetic field strengths of 86, 171, and 343 kA/m, respectively.[50] MR particle size, surface morphology, and intrinsic magnetic properties can affect the MR performance. In our system, we could neglect the effects of particle size, which can vary within 100 nm as a result of the coating process. The surface morphology was considered together with the intrinsic magnetic properties. The rough surfaces of MWCNT/PANI/CI particles enhanced the shear stress by promoting flocculation, as was observed in the absence of a magnetic field. However, the saturation magnetization of the MWCNT/PANI/CI particles was much lower than that of pure CI particles, which deteriorated the magnetic field response. Although the rough surface tended to influence the shear stress, the decrease in saturation magnetization resulted in the low shear stresses.

The above hypothesis was supported by the viscoelastic property measurements in an oscillatory test mode. A critical strain of 3×10^{-3}% determined from the amplitude sweep tests (see Figure S2 in the Supporting Information) was chosen to preserve the internal structure of the fluid. Frequency sweep experiments were performed on the two suspensions (containing MWCNT/PANI/CI particles or pure CI particles) at this strain under different magnetic fields strength. Figure 4b compares the storage modulus which was related with the strength of the chain structure as a function of frequency. In the absence of a magnetic field, the MWCNT/PANI/CI composite particle suspension displayed a higher storage modulus, indicating that the elastic properties originated from the chain structure, which was much stronger in the MWCNT/PANI/CI composite particle suspension than in the pure CI suspension. The rough surface of the MWCNT nest might delay slippage of the particles due to a high

flocculation force, even potentially forming unusual chainlike structure, which is usually observed for MR fluids under magnetic field. Under an external magnetic field, the pure CI suspension exhibited a slightly higher modulus because the high saturation magnetization between adjacent CI particles resulted in formation of more robust magnetic columns. Consequently, the elastic properties were much stronger in the CI suspension. The magnetic properties play a dominant role in the MR behavior. Changes in the elastic properties coincided with the flow curves.

After analyzing the effects of the coating structure on shear stress behavior, we investigated the dependence of the dynamic yield stress on the strength of the applied magnetic field. Just as a simple polarization model may be used to describe ER fluids, a magnetic model is appropriate for describing MR fluids. The magnetic-polarization model predicts a relationship between the field-dependent dynamic yield stress and the strength of the applied magnetic field as described below.[51,52]

Under a weak applied magnetic field, dynamic stress, τ_y, increases quadratically with increasing magnetic field strength, as shown in eq 1

$$\tau_y \propto H^2 \tag{1}$$

As the strength of the magnetic field is increased, local saturation in the magnetization becomes important, and τ_y may be expressed as

$$\tau_y = \sqrt{6}\phi\mu_0 M_S^{1/2} H^{3/2} \tag{2}$$

Here, M_s, μ_0, and φ are the local saturation of magnetization at its maximum value, the permeability of free space, and the volume fraction of the MR fluids, respectively.

At a high magnetic field, the magnetic saturation is present in all particles, and the yield stress and modulus do not respond to an external magnetic field

$$\tau_y^{sat} = 0.086\phi\mu_0 M_s^2 \tag{3}$$

Assuming that ER and MR fluids may be described in analogous ways, we propose the existence of a critical magnetic field strength (H_c) for MR fluids, which suggests a new universal relationship[53]

$$\tau_y(H_o) = \alpha {H_o}^2 \left(\frac{\tanh \sqrt{H_o/H_c}}{\sqrt{H_o/H_c}} \right) \tag{4}$$

Here, α is related to the susceptibility of the fluid, the volume fraction, and other analogous physical parameters. τ_y displays two limiting behaviors with respect to H_0

$$\tau_y = \alpha {H_o}^2 \text{ for } H_o << H_c \tag{5a}$$

$$\tau_y = \alpha\sqrt{H_c}{H_o}^{3/2} \text{ for } H_o >> H_c \tag{5b}$$

Figure 4c shows the replotted dynamic yield stress as a function of magnetic field strength for MWCNT/PANI/CI suspension. The data agreed well with eq 4, and H_c was 92.85 kA/m.

A generalized scaling relationship can be obtained by scaling eq 4 via H_c and $\tau_y(H_c) = 0.762\alpha {H_c}^2$ according to

$$\hat{\tau} = 1.313\hat{H}^{3/2}\tanh\sqrt{\hat{H}} \tag{6}$$

The data presented in Figure 4c collapsed onto a single curve upon application of eq 6, as demonstrated in Figure 4d.

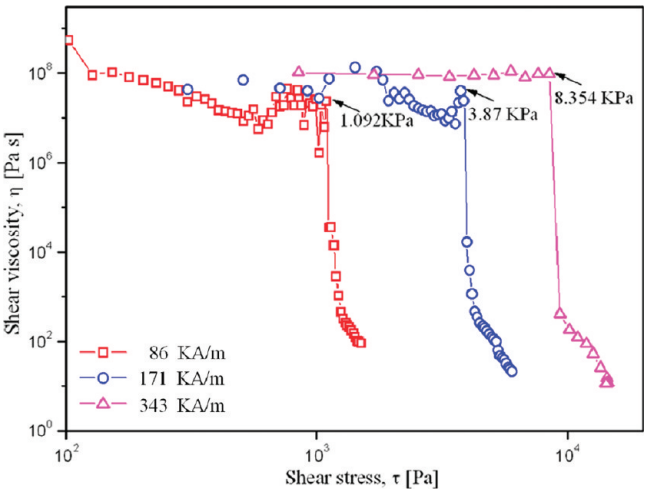

Figure 5. Shear viscosity vs shear stress obtained via controlled shear stress mode for MWCNT/PANI/CI suspension under different magnetic field strengths.

This observation suggests an interpretation that at high applied magnetic field strengths, the polarization force between the magnetic particles is enhanced and the magnetic particles mutually attract under the magnetic field due to the polarization force that favors formation of chain-like structures and robust columns. At a sufficiently high magnetic field, magnetic saturation occurs, and the force fails to increase with increasing magnetic field strength, and the exponent decreases from 2.0 to 1.5. The MR fluids display different behaviors, depending on the magnetic field strength.

In addition to the dynamic yield stress, the static yield stress was investigated. A controlled shear stress (CSS) was applied starting from a resting state and increasing to a critical stress, at which point the sample began to flow.[54] Figure 5 shows the shear viscosity as a function of the shear stress. The shear viscosity was constant at low shear stress, fell abruptly as the shear stress increased, and finally approached a constant value at high shear stress. Below a critical static yield stress, no macroscopic flow occurred. At the point marked with an arrow, all curves indicated a drop in the shear viscosity of greater than 6 orders of magnitude. This value represents a static yield stress of 1.092, 3.87, and 8.354 kPa, at different magnetic strength of 86, 171, and 343 KA/m, respectively. The sample did display a certain level of creep below this stress, but for our purposes, the behavior was assumed to be static. Compared to the dynamic yield stress, a slightly lower static yield stress was observed especially at 343 KA/m.

3.3. Sedimentation Stability. The sedimentation properties were investigated using a novel optical analyzer, a Turbiscan lab (Formulation, France) apparatus, which measures the dispersion state from light scattering data and derives the migration velocity or mean particles size of particles over time.[55] In a typical test, a particle suspension was transferred to a glass cylindrical cell and analyzed under illumination in the near-infrared (λ = 880 nm). The illumination beam scanned the sample cell (70 mm height, 27.5 mm external diameter) periodically from bottom to top. Two synchronous optical sensors measured the transmission (T) through the sample or the backscattering (BS) of light on the illumination side of the sample. Upon sedimentation of the particles, the transmission profile varied with the cell height over

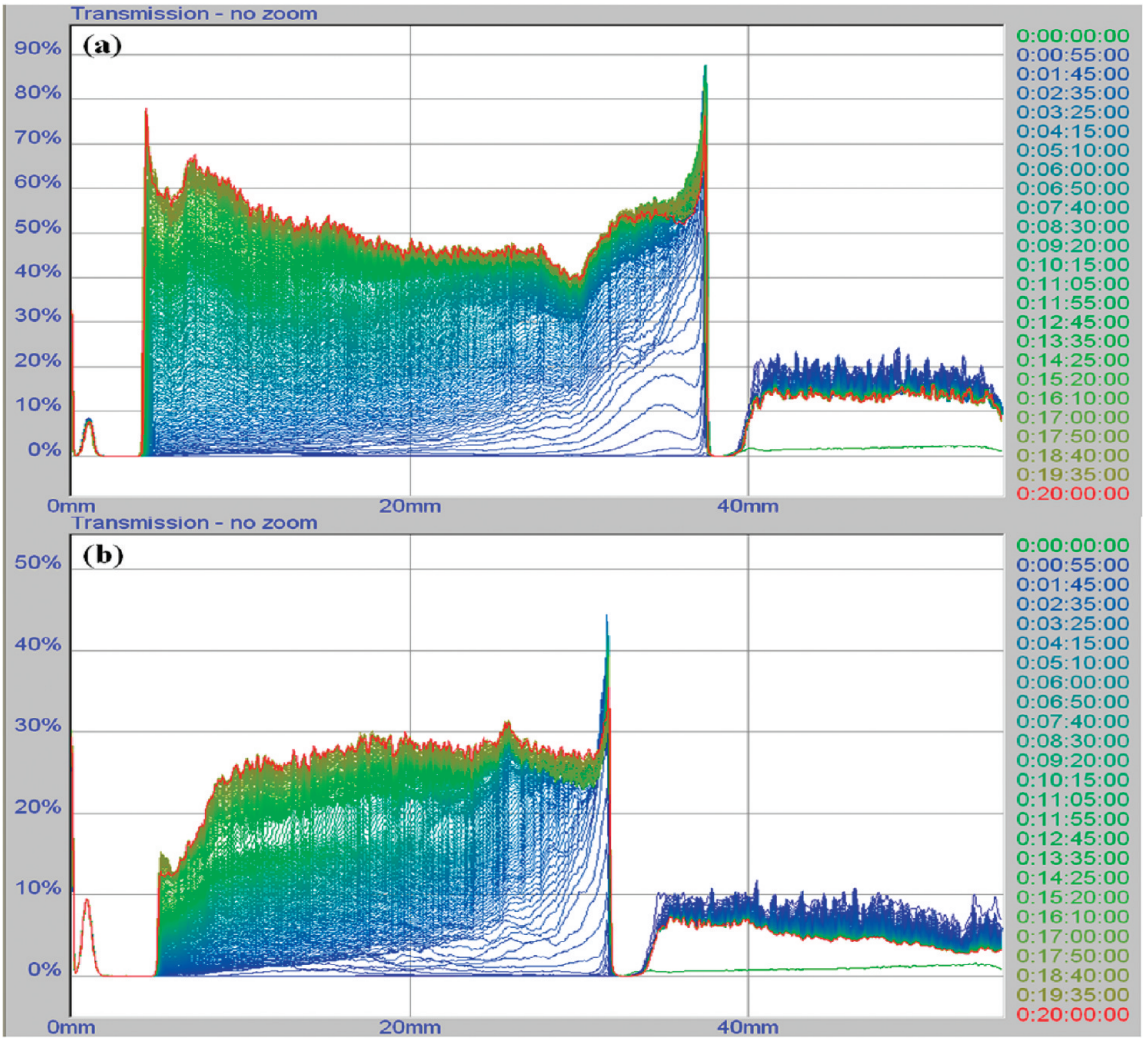

Figure 6. Typical turbiscan spectra of (a) pure CI suspension and (b) MWCNT/PANI/CI suspension.

time (see Figure S3 in the Supporting Information). Panels a and b in Figure 6 show typical transmission profiles obtained from the Turbiscan lab, each curve in which from top to bottom represents a scanning result at the corresponding time (hours:minutes: seconds:milliseconds) listed on the right side of the figures. The profiles indicate the percentage of light transmitted though the sample as a function of the height of the sample cell for a pure CI suspension and a MWCNT/PANI/CI suspension.[56] The *X* axis and *Y* axis in the transmission diagram represent the height of the sample cell and the variations in the transmitted light throughout the sample cell. The MWCNT/PANI/CI suspension displayed a lower transmission than the pure CI suspension. A well-dispersed suspension usually does not transmit much light, and the transmission measurement is very low. The low transmission of the MWCNT/PANI/CI suspension corresponded to a stable dispersion. The dispersion stability was monitored by measuring the transmission of the MR fluid sample contained cell at a fixed height as a function of time. As shown in Figure 7a, which was measured at the middle height point of the cell, both suspensions initially showed transmissions near zero because of the presence of a homogeneous dispersion. The transmission gradually increased over time due to settling. The transmission of the pure CI suspension was higher than that of the MWCNT/PANI/CI suspension during the full length of the test. The migration velocity (slope of the transmission as a function of time) for the CI suspension was much larger than that of the MWCNT/PANI/CI suspension. These results indicated that the MWCNT/PANI/CI suspension was more stable than the pure CI suspension.

We also examined the dispersion stability by observing the sedimentation ratio as a function of time as shown in Figure 7b. In this method, settling of the macroscopic phase boundary between the concentrated suspension and supernatant liquid was observed. Apparently, compared with pure CI suspension, MWCNT-coated PANI/CI particles indicate slow sedimentation velocity during the initial 5 h and then tend to get stable. In contrast with the pure CI suspension, the MWCNT-coated PANI/CI particles underwent slow sedimentation over 20 h. The turbiscan data of Figure 7a, combined with the sedimentation ratio of Figure 7b, indicated that the MWCNT-wrapped PANI/CI suspension formed a more stable dispersion than did the pure CI suspension. This stability was attributed to two properties, as shown in the inset photograph taken of Figure 7b. First, the coated MWCNT nest and the PANI shell produced a rough surface and decreased the density, thereby reducing the density mismatch with the oil (density: 0.96 g/cm^3). Thus,

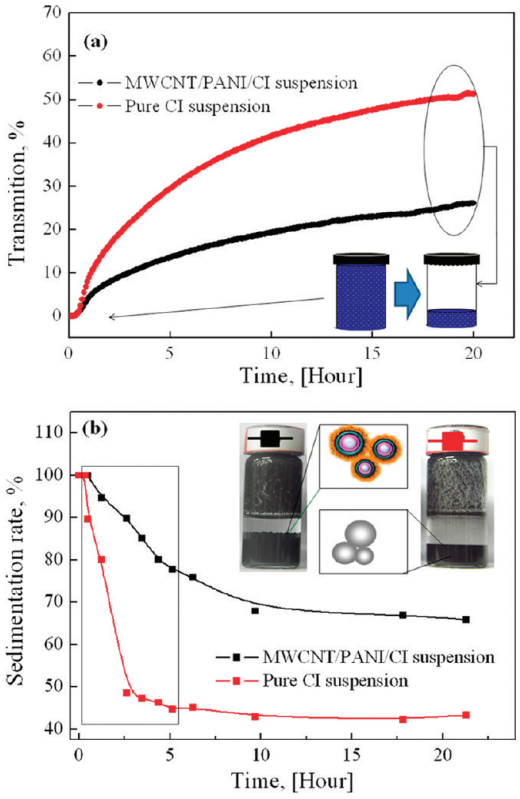

Figure 7. (a) Change of transmission as a function of time for (red) pure CI suspension and (black) MWCNT/PANI/CI suspension and (b) recorded sedimentation ratio as a function of time (red) pure CI suspension and (black) MWCNT/PANI/CI suspension; the inset images are snapshots taken after 20 h passed.

during particle migration, flocculation due to the rough surfaces delayed settling. Second, in contrast with the pure CI particles which are composed of an inorganic metal, the MWCNT/PANI/CI particles were wrapped by large PANI chains and MWCNTs. These organic surfaces may be more compatible with silicone oil, which possesses long and complex chains composed of alternating silicon and oxygen atoms (−Si−O−Si−O−Si−) or siloxane.[57] Furthermore, because of the conducting PANI and MWCNT coating, these particles could be also applied for ER materials.

4. CONCLUSIONS

In summary, this work attempted to reduce sedimentation in CI-based MR fluids by wrapping the CI particles in a PANI shell and a MWCNT nest via facile dispersion polymerization followed by solvent casting. The PANI shell formed a DBSA-doped emeraldine salt, as indicated by the Raman spectra, and the thickness was ca. 80 nm. The particle surfaces were rough due to a dense MWCNT nest. The coated CI particles displayed slightly lower MR performances under an applied magnetic field because of the weaker saturation magnetization, but the shear behavior was enhanced by flocculation due to the rough surface. The dynamic yield stress of the MWCNT/PANI/CI suspension depended on the magnetic field strength, and this relationship was analyzed using a universal yield stress correlation. The sedimentation rate decreased significantly because of the reduced density and the presence of rough surface morphologies. The synthesis of the PANI shell was insensitive to the use of vigorous stirring, which avoided CI particle sedimentation. The procedure for preparing the MWCNT nest was simple and reproducible. This novel core−shell structure with a low density and a rough surface improves the properties of MWCNT/PANI/CI particles for use in MR fluid applications.

■ ASSOCIATED CONTENT

Supporting Information. Figures including EDS spectra of PANI coated CI particles, amplitude sweep of the MR fluids and scan mode of Turbiscan lab. This information is available free of charge via the Internet at http://pubs.acs.org/.

■ AUTHOR INFORMATION

Corresponding Author
*E-mail: hjchoi@inha.ac.kr (H.J.C.); ysseo@snu.ac.kr (Y.S.).

■ ACKNOWLEDGMENT

The authors gratefully acknowledge Mr. Hwang Sun Jae for valuable assistance with the transmission electron microscopy (TEM) measurements. This study was supported by National Research Foundation, Korea ((43450-1, Choi) and (R11-2005-065, Seo)) and the Ministry of Knowledge and Economy (Fundamental R&D Program for Core Technology of Materials, RIAM 0427-20100043, Seo).

■ REFERENCES

(1) Alves, S.; Alcantara, M. R.; Neto, A. M. F. *J. Rheol.* **2009**, *53*, 651–662.
(2) Bombard, A. J. F.; Knobel, M.; Alcantara, M. R. *Int. J. Mod. Phys. B* **2007**, *21*, 4858–4867.
(3) de Vicente, J.; Klingenberg, D. J.; Hidalgo-Alvarez, R. *Soft Matter* **2011**, *7*, 3701–3710.
(4) Lopez-Lopez, M. T.; Zubarev, A. Y.; Bossis, G. *Soft Matter* **2010**, *6*, 4346–4349.
(5) Bica, I.; Choi, H. J. *Int. J. Mod. Phys. B* **2008**, *22*, 5041–5064.
(6) Park, B. J.; Fang, F. F.; Choi, H. J. *Soft Matter* **2010**, *6*, 5246–5253.
(7) Cheng, H. B.; Zuo, L.; Song, J. H.; Zhang, Q. J.; Wereley, N. M. *J. Appl. Phys.* **2010**, *107*, 09B507.
(8) Bica, I. *Mater. Lett.* **2009**, *63*, 2230–2232.
(9) Bica, I. *J. Ind. Eng. Chem.* **2010**, *16*, 359–363.
(10) Ulicny, J. C.; Snavely, K. S.; Golden, M. A.; Klingenberg, D. J. *Appl. Phys. Lett.* **2010**, *96*, 231903.
(11) Guerrero-Sanchez, C.; Lara-Ceniceros, T.; Jimenez-Regalado, E.; Rasa, M.; Schubert, U. S. *Adv. Mater.* **2007**, *19*, 1740–1747.
(12) Pu, H. T.; Jiang, F. J.; Yang, Z. L. *Mater. Lett.* **2006**, *60*, 94–97.
(13) Ramos, J.; de Vicente, J.; Hidalgo-Alvarez, R. *Langmuir* **2010**, *26*, 9334–9341.
(14) Jain, N.; Zhang, X.; Hawkett, B. S.; Warr, G. G. *ACS Appl. Mater. Interfaces* **2011**, *3*, 662–667.
(15) Lopez-Lopez, M. T.; Rodriguez-Arco, L.; Zubarev, A.; Iskakova, L.; Duran, J. D. G. *J. Appl. Phys.* **2010**, *108*, 083503.
(16) Viota, J. L.; de Vicente, J.; Duran, J. D. G.; Delgado, A. V. *J. Colloid Interface Sci.* **2005**, *284*, 527–541.
(17) McIntyre, E. C.; Oh, H. J.; Green, P. F. *ACS Appl. Mater. Interf.* **2010**, *2*, 965–968.
(18) Cheng, Y.; Wu, K.; Liu, F.; Guo, J.; Liu, X.; Xu, G.; Cui, P. *ACS Appl. Mater. Interf.* **2010**, *2*, 621–625.
(19) Choi, H. J.; Jhon, M. S. *Soft Matter* **2009**, *5*, 1562–1567.
(20) Zhang, X.; Peng, S.; Wen, W.; Li, W. *Smart Mater. Struct.* **2008**, *17*, 045001.

(21) Jung, H. J.; Lee, S. J.; Jang, D. D.; Kim, I. H.; Koo, J. H.; Khan, F. *IEEE Trans. Magn.* **2009**, *45*, 3930–3933.
(22) Jang, I. B.; Kim, H. B.; Lee, J. Y.; You, J. L.; Choi, H. J.; Jhon, M. S. *J. Appl. Phys.* **2005**, *97*, 10Q912.
(23) de Vicente, J.; Lopez-Lopez, M. T.; Duran, J. D. G.; Gonzalez-Caballero, F. *Rheol. Acta* **2004**, *44*, 94–103.
(24) Tang, X.; Zhang, X.; Tao, R.; Rong, Y. *J. Appl. Phys.* **2000**, *87*, 2634–2638.
(25) de Vicente, J.; Lopez-Lopez, M. T.; Gonzalez-Caballero, F.; Duran, J. D. G. *J. Rheol.* **2003**, *47*, 1093–1109.
(26) Zhang, X.; Li, W.; Gong, X. L. *Smart Mater. Struct.* **2008**, *17*, 015051.
(27) Lim, S. T.; Choi, H. J.; Jhon, M. S. *IEEE Trans. Magn.* **2005**, *41*, 3745–3747.
(28) Fang, F. F.; Jang, I. B.; Choi, H. J. *Diamond Relat. Mater.* **2007**, No. 16, 1167–1169.
(29) Guo, Z.; Henry, L. L.; Palshin, V.; Podlaha, E. J. *J. Mater. Chem.* **2006**, *16*, 1772–1777.
(30) Cho, M. S.; Lim, S. T.; Jang, I. B.; Choi, H. J.; Jhon, M. S. *IEEE Trans. Magn.* **2004**, *40*, 3036–3038.
(31) Fang, F. F.; Choi, H. J. *J. Appl. Phys.* **2008**, *103*, 07A301.
(32) Fang, F. F.; Choi, H. J.; Seo, Y. *ACS Appl. Mater. Interf.* **2010**, *2*, 54–60.
(33) Fang, F. F.; Choi, H. J.; Choi, W. S. *Colloid Polym. Sci.* **2010**, *288*, 359–363.
(34) Shin, K.; Park, Y. S.; Woo, J. W.; Whang, Y. A. *J. Korean Ind. Eng. Chem.* **2002**, *13*, 482–485.
(35) Barthet, C.; Armes, S. P.; Lascelles, S. F.; Luk, S. Y.; Stanley, H. M. E. *Langmuir* **1998**, *14*, 2032–2041.
(36) Cho, M. S.; Cho, Y. H.; Choi, H. J.; Jhon, M. S. *Langmuir* **2003**, *19*, 5875–5881.
(37) Jing, S.; Xing, S.; Dong, F.; Zhao, C. *Polym. Composite* **2008**, *29*, 1165–1168.
(38) Moulton, S. E.; Innis, P. C.; Kane-Maguire, L. A. P.; Ngamna, O.; Wallace, G. G. *Curr. Appl. Phys.* **2004**, *4*, 402–406.
(39) Haba, Y.; Segal, E.; Narkis, M.; Titelman, G. I.; Siegmann, A. *Synth. Met.* **2000**, *110*, 189–193.
(40) Segal, E.; Aviel, O.; Narkis, M. *Polym. Eng. Sci.* **2000**, *40*, 1915–1920.
(41) Kim, J. W.; Liu, F.; Choi, H. J. *J. Ind. Eng. Chem.* **2002**, *8*, 399–403.
(42) Li, W. G.; Wan, M. X. *J. Appl. Polym. Sci.* **1999**, *71*, 615–621.
(43) Yi, H.; Song, H.; Chen, X. *Langmuir* **2007**, *23*, 3199–3204.
(44) Do Nascimento, G. M.; Silva, C. H. B.; Izumi, C. M. S.; Temperini, M. L. A. *Spectrochim. Acta A* **2008**, *71*, 869–875.
(45) Yao, P.; Xu, J.; Wang, Y.; Zhu, C. *J. Mater. Sci: Mater. Electron.* **2009**, *20*, 891–898.
(46) Melo, L. O.; Ponzio, E. A.; Carmona-Ribeiro, A. M.; Torresi, R. M. *e-Polym.* **2008**, *149*, 1–13.
(47) Wereley, N. M.; Chaudhuri, A.; Yoo, J. H.; John, S.; Kotha, S.; Suggs, A.; Radhakrishnan, R.; Love, B. T.; Sudarshan, T. S. *J. Intell. Mater. Syst. Struct.* **2006**, *17*, 393–401.
(48) Rankin, P. J.; Horvath, A. T.; Klingenberg, D. J. *Rheol. Acta* **1999**, *38*, 471–477.
(49) Larson, R. G. In *The Structure and Rheology of Complex Fluids*; Oxford University Press: New York, 1999; Chapter 7, pp 337−349.
(50) Wollny, K.; Läuger, J.; Huck, S. *Appl. Rheol.* **2002**, *12*, 25–31.
(51) Ginder, J. M.; Davis, L. C.; Elie, L. D. *Int. J. Mod. Phys. B* **1996**, *10*, 3293–3303.
(52) Choi, H. J.; Cho, M. S.; Kim, J. W.; Kim, C. A.; Jhon, M. S. *Appl. Phys. Lett.* **2001**, *78*, 3806–3808.
(53) Fang, F. F.; Choi, H. J.; Jhon, M. S. *Colloids Surf., A: Physicochem. Eng. Aspect* **2009**, *351*, 46–51.
(54) de Vicente, J.; Vereda, F.; Segovia-Gutierrez, J. P.; del Puerto Morales, M.; Hidalgo-Alvarez, R. *J. Rheol.* **2010**, *54*, 1337–1362.
(55) Buron, H.; Mengual, O.; Meunier, G.; Cayre, I.; Snabre, P. *Polym. Int.* **2004**, *53*, 1205–1209.
(56) Hong, S.; Kim, M.; Hong, C.; Jung, D.; Shim, S. E. *Synth. Met.* **2008**, *158*, 900–907.
(57) Li, J.; Gong, X.; Zhu, H.; Jiang, W. *Polym. Test.* **2009**, *28*, 331–337.